Journal of Cellular Physiology



# Alternative Splicing of Nav1.5: An Electrophysiological Comparison of 'Neonatal' and 'Adult' Isoforms and Critical Involvement of a Lysine Residue

RUSTEM ONKAL,[1] JOANNA H. MATTIS,[1,2] SCOTT P. FRASER,[1] JAMES K.J. DISS,[1,3] DONGMIN SHAO,[1,4] KENJI OKUSE,[4] AND MUSTAFA B.A. DJAMGOZ[1]*

[1]*Division of Cell & Molecular Biology, Neuroscience Solutions to Cancer Research Group, Sir Alexander Fleming Building, South Kensington Campus, Imperial College London, London, UK*

[2]*Department of Molecular, Cellular & Developmental Biology, Yale University, New Haven, Connecticut*

[3]*Medical Molecular Biology Unit, Institute of Child Health, University College London, Guilford Street, London, UK*

[4]*Division of Cell & Molecular Biology, Molecular Neuroscience Group, Biochemistry Building, South Kensington Campus, Imperial College London, London, UK*

In developmentally regulated D1:S3 splicing of Nav1.5, there are 31 nucleotide differences between the 5′-exon ('neonatal') and the 3′-exon ('adult') forms, resulting in 7 amino acid differences in D1:S3-S3/S4 linker. In particular, splicing replaces a conserved negative aspartate residue in the 'adult' with a positive lysine. Here, 'neonatal' and 'adult' Nav1.5 α-subunit splice variants were stably transfected into EBNA-293 cells and their electrophysiological properties investigated by whole-cell patch-clamp recording. Compared with the 'adult' isoform, the 'neonatal' channel exhibited (1) a depolarized threshold of activation and voltage at which the current peaked; (2) much slower kinetics of activation and inactivation; (3) 50% greater transient charge ($Na^+$) influx; (4) a stronger voltage dependence of time to peak; and (5) a slower recovery from inactivation. Tetrodotoxin sensitivity and VGSCβ1-4 mRNA expression levels did not change. The significance of the charge-reversing aspartate to lysine substitution was investigated by mutating the lysine in the 'neonatal' channel back to aspartate. In this 'neonatal K211D' mutant, the electrophysiological parameters studied strongly shifted back towards the 'adult', that is the lysine residue was primarily responsible for the electrophysiological effects of Nav1.5 D1:S3 splicing. Taken together, these data suggest that the charge reversal in 'neonatal' Nav1.5 would (1) modify the channel kinetics and (2) prolong the resultant current, allowing greater intracellular $Na^+$ influx. Developmental and pathophysiological consequences of such differences are discussed.

J. Cell. Physiol. 216: 716–726, 2008. 

Voltage-gated $Na^+$ channels (VGSCs) open in response to membrane depolarization and allow rapid influx of $Na^+$. These large transmembrane proteins possess a central, pore-forming α-subunit (VGSCα), comprising four repeat domains (D1–D4), each composed of six membrane-spanning segments (S1–S6). Nine different VGSCα genes are found in higher vertebrates, each forming a channel with particular tetrodotoxin (TTX) sensitivity and variable electrophysiological properties (reviews: Catterall, 2000; Diss et al., 2004). TTX-sensitive VGSCαs (Nav1.1–1.4, 1.6, 1.7; $IC_{50} \sim 10$s nM) generally activate at around −40 mV and have fast inactivation kinetics, whereas TTX-resistant VGSCαs (Nav1.5, 1.8, 1.9; $IC_{50} \sim \mu M$) activate at more hyperpolarized potentials and inactivate much more slowly. VGSCα properties can also be more finely modulated in a subtype specific manner by association with one or more smaller accessory β-subunits (VGSC β1–4), typically altering voltage dependence of activation/inactivation, and increasing the level of functional channel density in the plasma membrane by promoting the intracellular trafficking of the mature protein and/or by enhancing the cell surface stability of VGSCαs via association with cytoskeletal elements such as ankyrin (Isom et al., 1994; Catterall, 2000; Isom, 2001; Diss et al., 2007).

Further VGSCα diversity can be generated at transcriptional, pre-translational and post-translational levels (review: Diss et al., 2004). In particular, alternative splicing has become an increasingly important mechanism for generating variation amongst VGSCαs (Gustafson et al., 1993; Klugbauer et al., 1995; Schaller et al., 1995; Dietrich et al., 1998; Plummer et al., 1998; Raymond et al., 2004). However, its electrophysiological

*Abbreviations*: TTX, tetrodotoxin; VGSC, voltage-gated sodium channel; VGPS, voltage-gated potassium channel; D1:S3, domain 1: segment 3; MPS, mammalian physiological saline; SEM, standard error of mean; $Q_{total}$, total charge; $V_{thres}$, threshold voltage for activation; $V_{peak}$, voltage for current peak; $V_{1/2}$, half activation/inactivation voltage; k, slope factor; $V_0$, voltage dependency of time to peak; $T_{peak}$, time to peak; $\tau_{f/s}$, fast/slow time constant of inactivation; τ, time constant for recovery from inactivation; $C_t$, threshold amplification cycle; AP, action potential.

Contract grant sponsor: The Pro Cancer Research Fund (PCRF).

*Correspondence to: Mustafa B.A. Djamgoz, Division of Cell & Molecular Biology, Neuroscience Solutions to Cancer Research Group, Sir Alexander Fleming Building, South Kensington Campus, Imperial College London, London SW7 2AZ, UK.
E-mail: m.djamgoz@imperial.ac.uk

Received 9 May 2007; Accepted 13 February 2008

DOI: 10.1002/jcp.21451

consequences have not yet been extensively investigated (review: Diss et al., 2004). A major type of alternative splicing of VGSCα genes in higher vertebrates involves inclusion of two alternative exons (5′ genomic and the 3′ genomic) encoding the D1:S3 segment and the D1:S3/S4 extracellular linker (Fig. 1A). These two exon 6 alternatives are distinguished by the presence (3′-exon) or absence (5′-exon) at position 7 (in the S3/S4 linker) of an aspartate residue. To date, D1:S3 splicing has been shown to occur in six of the nine VGSCαs (Nav1.1, 1.2, 1.3, 1.5, 1.6 and 1.7; review: Diss et al., 2004). This splicing was first described for Nav1.2 and Nav1.3 in rat brain and was deemed to be developmentally regulated since transcripts possessing the D1:S3 5′-exon were relatively abundant at birth but were quickly replaced by 3′-exon containing transcripts within a few days (Sarao et al., 1991; Gustafson et al., 1993). Consequently, the 5′-exon is termed 'neonatal' and the 3′-exon 'adult.'

We recently identified the 'neonatal' splice variant of Nav1.5 in metastatic breast cancer cells (Fraser et al., 2005; Chioni et al., 2005; Brackenbury et al., 2007). In most VGSCα genes, alternate D1:S3 exons differ at 19–21 nucleotides but the subsequent proteins differ by only one amino acid. Nav1.5 D1:S3 splicing is unusual in that the 5′-exon has 31 nucleotide differences from the 3′-exon form, resulting in 7 amino acid substitutions in D1:S3 and the S3/S4 linker of the VGSCα protein (Gellens et al., 1992; Chioni et al., 2005; Fraser et al., 2005) (Fig. 1B,C). Importantly, the 7 amino acid differences between the 'adult' and 'neonatal' splice isoforms were sufficient to generate a polyclonal antibody (NESOpAb) that recognized 'neonatal' Nav1.5 with ~400× selectivity over 'adult' Nav1.5, when tested on EBNA-293 cells expressing either of these Nav1.5 splice variants (Chioni et al., 2005). Of potential significance is the replacement of the negatively charged aspartate at position 211 in the 3′-exon with a positively charged lysine residue, and not a non-charged amino acid as for the other D1:S3 VGSCα spliced genes (Fig. 1B). This aspartate to lysine amino acid substitution leads to a charge-reversal towards positivity in the 'neonatal' Nav1.5 channel in a region adjacent to the S4 voltage sensor of domain 1 (Fig. 1C). Introduction of extra positive electrostatic potential to the S3–S4 linker region could lead to changes in Nav1.5 channel kinetics (Sheets and Hanck, 2002; McNulty et al., 2007). The effect of D1:S3 splicing on VGSC function has not been fully elucidated, but its conservation across VGSCα genes and species would indicate that it is likely to be significant. A previous investigation of single amino acid substitutions in the D1:S3 region of Nav1.2 found only limited effects (Auld et al., 1990). More recently, Ou et al. (2005) studied expression of the 'neonatal' splice form of Nav1.5 (termed hNbR1), taken from human neuroblastoma cells, but a direct electrophysiological comparison with the 'adult' splice form was not made.

The aims of the present study were to elucidate, for the first time (i) the possible electrophysiological differences between 'neonatal' and 'adult' exon-containing Nav1.5 VGSCαs, and (ii) the extent to which the key aspartate ('adult') to lysine ('neonatal') amino acid change contributes to any such electrophysiological difference. 'Neonatal', 'adult' and 'neonatal K211D' variants of Nav1.5 α-subunit were stably transfected into EBNA-293 cells and their electrophysiological properties were investigated by whole-cell patch-clamp recording in a comparative approach. Given that VGSCβ expression can modify VGSCα/Nav1.5 channel gating (Xiao et al., 2000; Fahmi et al., 2001), endogeneous VGSCβ mRNA levels were also measured by real-time PCR.

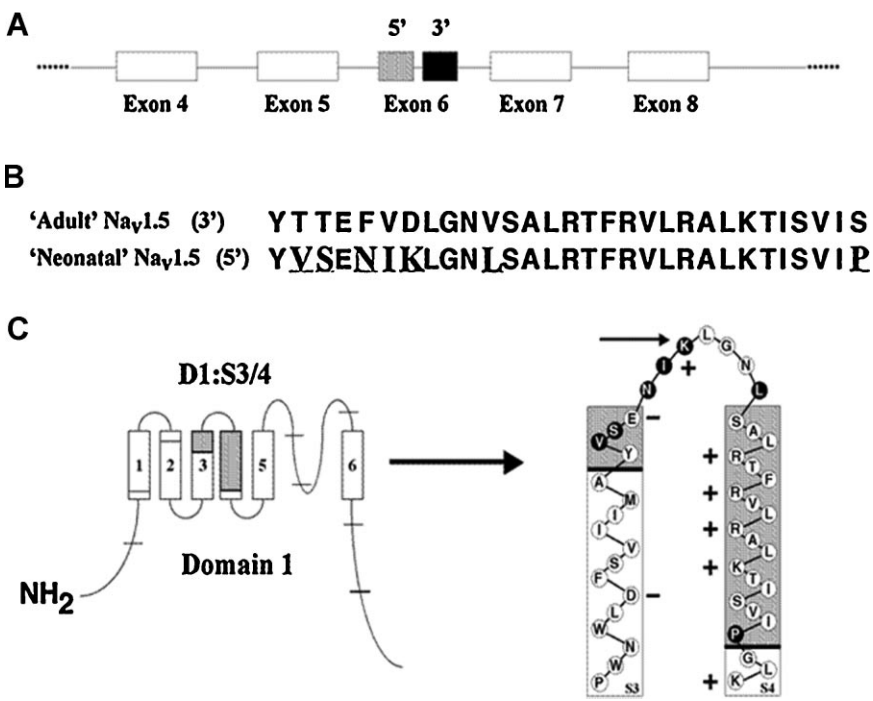


**Fig. 1. Molecular differences between 'neonatal' and 'adult' Nav1.5. A: Schematic diagram of the *SCN5A* gene encoding Nav1.5 showing the relative positions of the 5' ('neonatal': shaded) and 3' ('adult': black) exon 6. B: Deduced amino acid sequences of Nav1.5 exon 6 alternatives, with changed amino acids underlined. C: Location of the splicing is the S3 and S4 regions of domain (D1) of the protein, including the extracellular S3–4 linker (shaded area). The sequence differences between the two isoforms (black circles/white lettering) are located mainly in the C-terminal end of D1:S3 and the S3/S4 linker region of the channel, close to the four positively charged residues of the voltage-sensing S4. Small arrow indicates the "charge-reversing" amino acid change (i.e. negative aspartate in 'adult' to positive lysine in 'neonatal' exon 6).**

## Materials and Methods

### Cell culture

Modified human embryonic kidney cells (EBNA-293) stably transfected with various isoforms of Nav1.5 α-subunit (see below) were grown and maintained in minimum essential medium (MEM; with Earle's salts and glutamine) supplemented with 10 % fetal bovine serum (FBS) and 1 % non-essential amino acids. The growth media was also supplemented with 500 μg/ml Hygromycin B (Invitrogen, Paisley, UK) to select for stably transfected cells. Weakly metastatic breast cancer (MCF-7) and strongly metastatic prostate cancer (PC-3M) cells were cultured as described previously (Fraser et al., 2005; Mycielska et al., 2005). All cells were seeded into 100 mm Falcon tissue culture dishes (Becton Dickinson Ltd., Plymouth, UK) and grown in an incubator at 37°C, 100% humidity and 5% $CO_2$.

### K211D mutagenesis in 'neonatal' Nav1.5

Site-directed mutagenesis was performed on 'neonatal' Nav1.5 pcDNA (Chioni et al., 2005), substituting two key nucleotides in order to generate an expression vector for 'neonatal K211D' Nav1.5 (amino acid at position 211: lysine → aspartate) (Fig. 1B,C). The mutagenesis was performed using Quickchange® XL Site-Directed mutagenesis Kit (QCXLM; Stratagene, La Jolla, CA), according to manufacturer's instructions. The following primer pair (MWG Biotech) was used for the PCR reaction:

Forward: 5′-CATGGCATACGTATCTGAAAATATA-GACCTGGGCAATCTCTCAGC-3′
Reverse: 5′-GCTGAGAGATTGCCCAGGTCTATATTTTCAGA-TACGTATGCCATG-3′.

Following the PCR, reaction mixture was digested with *DpnI* restriction enzyme (10 U at 37°C for 1 h), and 3 μl of digested PCR mixture was transformed into ultra-competent XL10-Gold cells (Stratagene). Bacterial clones were then picked and the plasmid DNA was purified using a miniprep Kit (Qiagen, West Sussex, UK) followed by digestion with *Hind III* (Promega, Madison, WI). Clones were then sequenced (MWG Biotech, Ebersberg, Germany) to confirm the success of the mutagenesis.

### Transfection of EBNA-293 cells with 'adult', 'neonatal' and 'neonatal K211D' Nav1.5

The basic procedure was described previously (Chioni et al., 2005). Briefly, the 'adult' Nav1.5, cloned into plasmid pcDNA3.1, was transfected into EBNA-293 cells using Lipofectamine (Invitrogen) (Chandra et al., 1998). This cell line was a kind gift from Prof. Augustus Grant. 'Neonatal' Nav1.5, derived from site-directed mutagenesis of 'adult' Nav1.5 pcDNA, was transfected similarly (Chioni et al., 2005). For the 'neonatal K211D' Nav1.5 pcDNA transfections, performed for the first time, EBNA-293 cells were plated and grown to 80% confluence in 100 mm Falcon tissue culture dishes (Becton Dickinson Ltd.) for 24 h. For transfection, 15 μg 'neonatal K211D' Nav1.5 pcDNA and 25 μl of Lipofectamine 2000 (Invitrogen) were used. The cells were split (1:5) 24 h after the transfection and were selected using 500 μg/ml HygromycinB (Invitrogen) 24 h later. Individual colonies were picked after 2 weeks and tested for functional VGSC expression by whole-cell patch-clamp recording.

### Real-time PCR

Extraction of total RNA, synthesis of cDNA and real-time PCR utilizing SYBR I Green technology (Qiagen) were performed as described previously (Diss et al., 2005; Mycielska et al., 2005). β-actin was used as the internal normalizing gene (Diss et al., 2007). The following primer pairs (MWG Biotech) and annealing temperatures (°C) were used (Diss et al., 2007):

(1) β-actin: 5′-ATGGATGATGATATCGCCGC-3′ and 5′-ATCTTCTCGCGGTTGGCCTT-3′; (59°C).
(2) VGSC β1: 5′-AGAAGGGCACTGAGGAGTTT-3′ and 5′-GCAGCGATCTTCTTGTAGCA-3'; (60°C).
(3) VGSC β2: 5′-GAGATGTTCCTCCAGTTCCG-3′ and 5′-TGACCACCATCAGCACCAAG-3′; (62°C).
(4) VGSC β3: 5′-CTGGCTTCTCTCGTGCTTAT-3′ and 5′-TCAAACTCCCGGGACACATT-3′; (60°C).
(5) VGSC β4: 5′-TAACCCTGTCGCTGGAGGTG-3′ and 5′-TGAGGATGAGGAGCCCGATG-3′; (64°C).

PCR reactions were carried out in triplicates for both the target genes (VGSCβ1–4) and the control/normalizing gene (β-actin) in 'adult' and 'neonatal' Nav1.5 transfected EBNA-293 cells. The threshold amplification cycles ($C_t$), where the product fluorescence was greater than background noise, was determined for each reaction using Opticon Monitor 2 software (MJ Research, Hemel Hempstead, UK). The values for $C_t$ were then analysed by the $2^{-\Delta\Delta C_t}$ method (Livak and Schmittgen, 2001) to determine target gene expression levels, which were expressed as mean percentages (relative to the level in 'neonatal' EBNA-293 cells) ± standard errors (SEM) ($n \geq 3$). Each set of reactions also included a standard calibration curve for each target gene using five serial dilutions of the cDNA template (covering several orders of magnitude range) to confirm that the amplification efficiencies of the target and normalizing genes were approximately equal (data not shown), validating the $2^{-\Delta\Delta C_t}$ method (Livak and Schmittgen, 2001). Blank reactions, with sterile distilled $H_2O$ instead of cDNA, were performed in order control for any cross-contamination from other sources. Molecular weights of PCR products were verified by agarose gel electrophoresis.

### Electrophysiology

Standard whole-cell patch-clamp techniques were used as described previously (Grimes et al., 1995; Fraser et al., 2005). In voltage-clamp recordings, in order to study voltage-gated $Na^+$ currents in isolation, $K^+$ channels were blocked by replacing KCl with CsCl in the pipette solution. Thus, the patch pipette solution contained (in mM): CsCl 145; NaCl 5; $MgCl_2$ 2; $CaCl_2$ 1; EGTA 11 and HEPES 10 (pH 7.2, adjusted with CsOH). The extracellular mammalian physiological saline (MPS) solution contained (in mM): NaCl 144; KCl 5.4; $MgCl_2$ 1; $CaCl_2$ 2.5; HEPES 5 and glucose 5.6 (pH 7.3, adjusted with NaOH). Sodium-free MPS contained equimolar choline chloride for sodium chloride. All solutions were bath-applied during patch-clamp recordings.

Patch pipettes were made from borosilicate glass (GC100-F; Harvard Apparatus Ltd., Kent, UK) using a two-stage vertical puller (Narishige, Tokyo, Japan) and heat-polished to resistances of 5–10 MΩ when filled with an internal patch solution. Cells were viewed using an inverted microscope (IM35; Zeiss, Thornwood, NY). Membrane currents/voltages were recorded with an Axopatch 200B (Axon Instruments, Foster City, CA) and sampled at 50 kHz with a 5 kHz low-pass Bessel filter. The DC offset resulting from the junction potential was nulled and series resistance was compensated by at least 80%; capacitative transients in voltage-clamp recordings were compensated using standard techniques. Data were stored and analysed using pCLAMP software (Axon Instruments). All recordings were performed at room temperature and only small cells that appeared isolated in culture were used. In order to avoid possible contamination from endogenous $Na^+$ currents and to minimize series resistance error, only cells with peak current amplitudes in the range 1,000–5,000 pA were used. Recordings were accepted only when seal resistances were more than 500 MΩ and the series resistance (less than 25 MΩ) changed less than 20% throughout the experiment. Data, obtained from at least 20 cells per condition, from a minimum of three separate dishes, were combined to give overall mean ± standard errors (SEM).

### Voltage-clamp protocols

A holding potential of −100 mV was used and four main types of command voltage protocols were applied, as follows:

(1) *Standard current-voltage (I–V) protocol*: This was used to determine voltage dependence and kinetics (i.e. time to peak) of activation and kinetics of inactivation (i.e. slow and fast constants of current decay from peak). The currents were generated by pulsing the membrane potential for 60 msec to, between −80 and +45 mV, in 5 mV increments, with an interpulse duration of 2 sec.
(2) *Steady-state inactivation protocol*: This was used to study the voltage dependence of inactivation at steady state. Recordings were made using prepulses to −130 mV to −10 mV, in 10 mV increments, for 1 sec, followed immediately by an 80 msec test pulse to −10 mV, with an interpulse duration of 2 sec.
(3) *The time course of recovery from inactivation protocol*: Recovery from inactivation was studied using a double-pulse protocol. Cells were treated with an 80 msec 'control pulse' to −10 mV (giving current $I_c$), returned to the holding potential and then an identical 'test pulse' was applied (giving current $I_t$) at time intervals increasing from 5 to 155 msec in 10 msec increments.
(4) *Tetrodotoxin (TTX) protocol*: An initial control pulse of 80 msec duration was applied to −10 mV whilst the cell was perfused in normal MPS. TTX (0.1–10 μM; Alomone) was applied to the cell for 1 min and then the test pulse to −10 mV was repeated. Finally, the perfusion was returned to control solution and after 1 min, a third test pulse was applied to determine whether the effect of TTX was reversible.

### Curve fitting

Conductance-voltage relationships were computed using the equation: $G = I/(V - V_{rev})$, where G is the conductance; I the current amplitude; V the test pulse; and $V_{rev}$ the theoretical $Na^+$ reversal potential, as calculated from the Nernst equation. Normalized conductance-voltage (G−V) curves for voltage dependence of steady-state activation and inactivation were fitted to a Boltzmann function of the form:

$$G = G_{max}/[1 - \exp(V_m - V_{1/2})/k] \quad (1)$$

where $G_{max}$ is the maximal conductance; $V_m$ is the membrane voltage; $V_{1/2}$ is the voltage at which the current is half activated/inactivated, and k is the slope factor of voltage sensitivity. The voltage-dependence of time to peak and the time course of inactivation (i.e. decay of current) were fitted to the following single- and double-exponential decay functions, respectively:

$$\tau = A_1 + A_2\exp(-V/V_0) \quad (2)$$

$$I = A_f\exp(-t/\tau_f) + A_s\exp(-t/\tau_s) + C \quad (3)$$

where $A_1$ and $A_2$ are the coefficients of decline of the time constant, τ with voltage, V is the membrane potential and $V_0$ is a constant describing the voltage dependence of τ. For the double-exponential equation, $A_s$ and $A_f$ are the maximal amplitudes of the slow and fast components of the total current and $\tau_s$ and $\tau_f$ are the time constants for decay of the slow and fast components of the current, respectively; and the constant C is the asymptote. In order to analyse the time course of recovery from inactivation, $I_t/I_c$ (see above) was plotted as a function of recovery time (Δt) and fitted to a single exponential function.

The total charge (Coulomb × $10^{-15}$) entry into the cell ($Q_{total}$) at each test voltage was calculated manually as the area under the recorded current trace, divided into 0.02 msec wide 'columns', for the period 0.5 to 30 msec, following the onset of the command voltage:

$$Q_{total} = \Sigma(I \times 0.02) \quad (4)$$

where I (in pA) is the value of the instantaneous current at the right hand side of each current column. For every recording used for this analysis: (i) maximal currents were very similar, between 2340 and 2380 pA; and (ii) peak current amplitudes at given command voltages were also similar to within ±5 % (n = 5 cells each). Data were presented as the percentage difference in $Q_{total}$ ($\Delta Q_{total}$) between 'neonatal' and 'adult' Nav1.5 recordings at corresponding membrane voltages.

### Data analysis

All quantitative data are presented as mean ± standard errors (SEM), unless stated otherwise. For whole-cell patch-clamp data, pairwise statistical significance was determined with Student's unpaired t-test. Real-time PCR data was analysed using the $2^{-\Delta\Delta C_t}$ method (Livak and Schmittgen, 2001), and compared with Student's paired/unpaired *t*-test or one way analyses of variance (ANOVA) followed by Newman-Keuls post hoc analyses, as appropriate. Results were considered significant at $P < 0.05$ (*) and highly significant at $P < 0.01$ (**).

## Results

Non-transfected EBNA-293 cells expressed endogenous inward currents of only ~4 pA/pF and only infrequently. Upon depolarization, EBNA-293 cells transfected with either 'adult'

TABLE 1. Summary of electrophysiological data obtained from EBNA-293 cells transfected with either 'adult', 'neonatal' or 'neonatal K211D' forms of Nav1.5 (means ± SEM), n ≥ 20

| (#) Parameter | 'Adult' Nav1.5 | 'Neonatal' Nav1.5 | 'Neonatal K211D' | Significance (*P* values) |
|---|---|---|---|---|
| (1) $V_{thres}$ (mV) | −61.5 ± 0.4 | −59.7 ± 0.4 | −62.8 ± 0.5 | a**, c** |
| (2) $V_{peak}$ (mV) | −19.7 ± 0.8 | −12.2 ± 0.8 | −23.2 ± 1.0 | a**, b*, c** |
| (3) Activation $V_{1/2}$ (mV) | −39.3 ± 0.2 | −33.3 ± 0.3 | −40.9 ± 0.2 | a**, b**, c** |
| (4) Activation k | 6.2 ± 0.2 | 7.6 ± 0.3 | 5.6 ± 0.2 | a**, b*, c** |
| (5) Inactivation $V_{1/2}$ (mV) | −93.2 ± 0.2 | −95.0 ± 0.2 | −93.5 ± 0.3 | a**, c** |
| (6) Inactivation k | −6.6 ± 0.2 | −6.9 ± 0.2 | −6.7 ± 0.2 | — |
| (7) $V_0$ (mV) | 16.2 ± 0.2 | 19.6 ± 0.2 | 15.0 ± 0.4 | a**, b*, c** |
| (8) $T_{peak}$ at −20 mV (msec) | 0.86 ± 0.02 | 1.01 ± 0.02 | 0.81 ± 0.02 | a**, b*, c** |
| (9) $\tau_f$ at −20 mV (msec) | 1.01 ± 0.03 | 1.18 ± 0.03 | 0.91 ± 0.02 | a**, b*, c** |
| (10) $\tau_s$ at −20 mV (msec) | 5.65 ± 0.15 | 6.84 ± 0.24 | 5.39 ± 0.14 | a**, c** |
| (11) (τ) (msec) | 31.2 ± 1.0 | 38.6 ± 0.9 | 25.9 ± 1.1 | a**, b**, c** |

$V_{thres}$, threshold voltage for activation; $V_{peak}$, voltage at which current was maximal; $V_{1/2}$, half-maximal voltage; k, slope factor (i.e. voltage sensitivity); $V_0$, coefficient describing the voltage-dependence of time to peak; $t_p$, time to peak; $\tau_f$, 'fast' inactivation constant; $\tau_s$, 'slow' inactivation constant; τ, recovery from inactivation time constant. "a" denotes comparison between 'adult' and 'neonatal'; "b" denotes comparison between 'adult' and 'neonatal K211D'; "c" denotes comparison between 'neonatal' and 'neonatal K211D'. Statistical comparisons were made using unpaired Student's *t* tests. Significance $^*P < 0.05$ and $^{**}P < 0.01$.

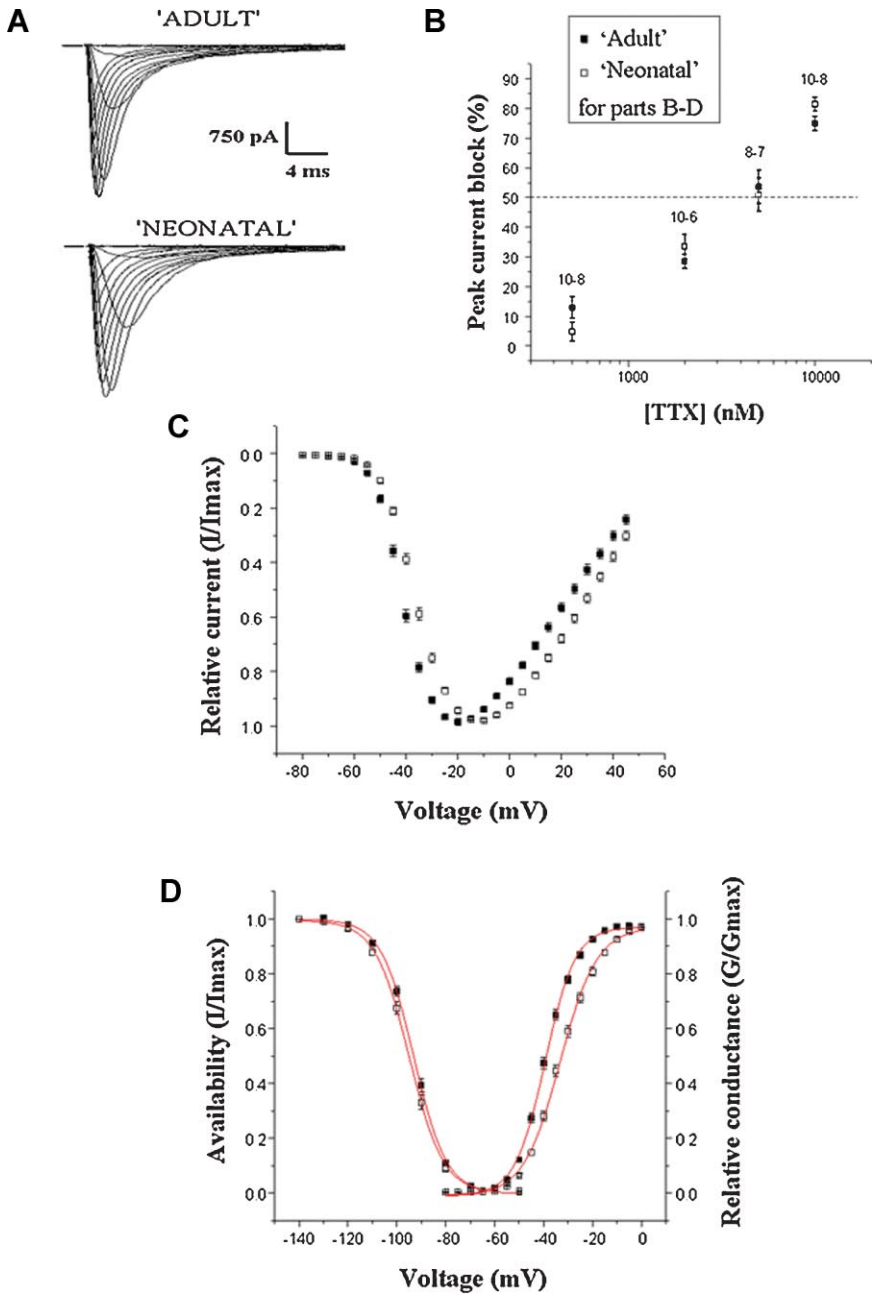


**Fig. 2. Voltage dependence of activation and inactivation. A: Representative VGSC currents recordings from standard I–V protocol in EBNA-293 cells transfected with 'adult' or 'neonatal' Nav1.5. For clarity, only every second current trace generated is displayed. Outward ($K^+$) currents were blocked by including $Cs^+$ in the internal pipette solution. B: Dose-response data for the effects of TTX on 'adult' and 'neonatal' Nav1.5, showing the percentage maximal reduction of the peak current (elicited by pulsing to −10mV) following drug application. Given on top of the data points are the (n) numbers for 'adult' and 'neonatal' recordings, respectively. C: Normalized peak current versus voltage curves obtained from standard I–V protocol and (D) voltage-dependence of activation and inactivation. Activation conductance and steady state inactivation (availability) were fitted to standard Boltzmann functions. Data are presented as mean ± SEM ($n \geq 27$).**

or 'neonatal' Nav1.5 generated large (~200 pA/pF), rapidly activating inward currents (Fig. 2A). These currents were eliminated in a $Na^+$-free MPS solution, and substituting $CaCl_2$ for $BaCl_2$ in MPS had no effect (not shown), that is the currents were carried by $Na^+$. Furthermore, the currents were suppressed by TTX (Alomone, Jerusalem, Israel) with an $IC_{50}$ of ~5 μM for both splice variants (Fig. 2B). The values and statistical comparisons of the electrophysiological parameters measured are summarized in Table 1.

### Voltage dependence of activation and inactivation

Current-voltage (I–V) relationships showed that the 'adult' and 'neonatal' splice forms of Nav1.5 activated at $-61.5 \pm 0.4$ and $-59.7 \pm 0.4$ mV ($P < 0.01$, n = 43–37) and peaked at $-19.7 \pm 0.8$ and $-12.2 \pm 0.8$ mV, respectively ($P < 0.01$, n = 43–37) (Fig. 2C; Table 1). The normalized conductance-voltage (G–V) relationships gave half-activation voltage ($V_{1/2}$) values for the 'adult' and 'neonatal' splice forms of $-39.3 \pm 0.2$

and $-33.3 \pm 0.3$ mV, respectively ($P < 0.01$, n = 43–37), whilst the slope factor k was $6.2 \pm 0.2$ and $7.6 \pm 0.3$ mV per e-fold increase in $Na^+$ conductance, respectively ($P < 0.01$, n = 43–37) (Fig. 2D; Table 1). Voltages for steady-state half-inactivation ($V_{1/2}$) were $-93.2 \pm 0.2$ and $-95.0 \pm 0.2$ mV ($P < 0.01$, n = 27 each) whilst the slope factor k values were $-6.6 \pm 0.2$ and $-6.9 \pm 0.2$ mV per e-fold increase in $Na^+$ conductance for the 'adult' and 'neonatal' splice forms, respectively ($P = 0.21$, n = 27 each) (Fig. 2D; Table 1).

### Kinetics of activation and inactivation

The 'adult' and 'neonatal' Nav1.5 also differed significantly in their kinetics of activation and inactivation (Fig. 3A; Table 1). For

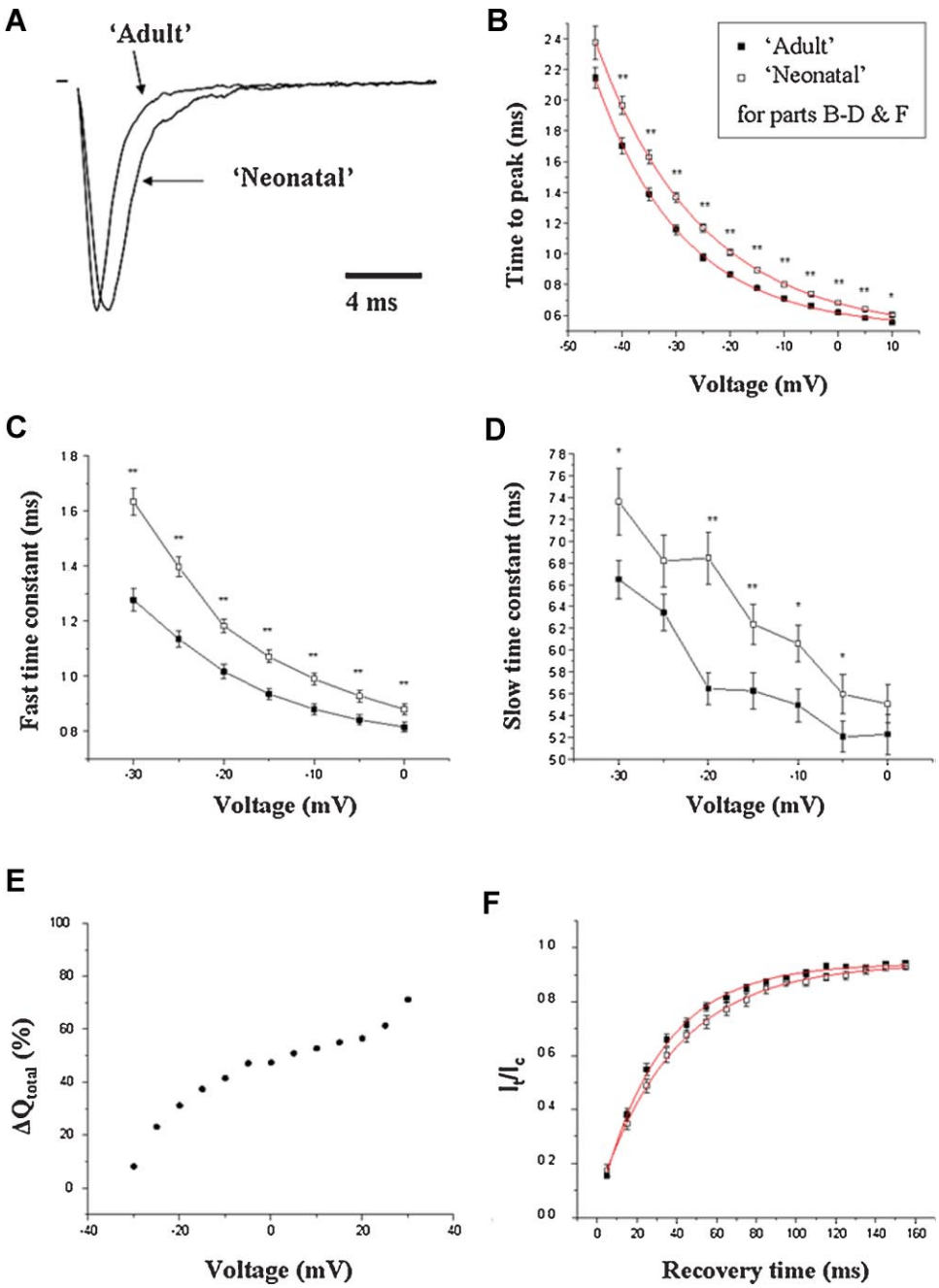


**Fig. 3. Kinetics of activation and inactivation. A: Traces of typical whole-cell VGSC (Nav1.5) currents (normalized for equal amplitude) from 'neonatal' and 'adult' splice forms elicited by 60 msec pulses to −25 mV. B: Time to peak, obtained from standard I–V protocol, as a function of test potential and fitted to a single order exponential function. C,D: The fast ($\tau_f$) and slow ($\tau_s$) time constants of inactivation as determined by fitting decaying current curves obtained from the I–V protocol to a double-exponential function. E: Percentage increase in total charge influx ($Q_{total}$) that passes across the membrane of 'neonatal' EBNA-293 cells relative to the 'adult' cells (for the time period 0.5–30 msec) plotted as a function of test potential. F: Time course of recovery from inactivation. Remaining current ($I_t/I_c$) was plotted as a function of recovery time (Δt), and fitted to a single exponential function. Data are presented as mean ± SEM (n ≥ 20; Table 1). Significance $^*P < 0.05$ and $^{**}P < 0.01$; unpaired Student's *t*-test.**

both splice forms, time to peak ($T_{peak}$) decayed exponentially with membrane voltage over the voltage range −45 to +10 mV (Fig. 3B). However, over the voltage range tested, 'neonatal' Nav1.5 reached peak current significantly more slowly than the 'adult' isoform. For example, at −20 mV, average times to peak for 'adult' and 'neonatal' were 0.86 ± 0.02 and 1.01 ± 0.02 msec, respectively ($P < 0.01$, n = 43–37) (Fig. 3B; Table 1). Moreover, the coefficients describing voltage dependence of $T_{peak}$ were also significantly different: 16.2 ± 0.2 mV for the 'adult' and 19.6 ± 0.2 mV for the 'neonatal' ($P < 0.01$, n = 43–37) per e-fold decrease in time to peak (Fig. 3B).

The kinetics of inactivation were analysed with the data obtained from the standard I–V protocol for depolarisations in the experimental range −30 to 0 mV (Fig. 3C,D). Current decays were best fit with a double-exponential decay function in ~95% of both 'adult' (n = 279) and 'neonatal' cases (n = 256). The average values of the time constants for fast inactivation ($\tau_f$) and slow inactivation ($\tau_s$) were plotted as a function of membrane potential (Fig. 3C,D). The $\tau_f$ values for depolarisations from −30 mV to 0 mV were significantly smaller for the 'adult' compared with the 'neonatal' splice form (Fig. 3C). For example, at −20 mV, the values of $\tau_f$ were 1.01 ± 0.03 msec for 'adult' and 1.18 ± 0.03 msec for 'neonatal' ($P < 0.01$, n = 43–37) (Table 1). The average values of $\tau_s$ were also significantly smaller for the 'adult' compared with the 'neonatal' splice form (Fig. 3D). At −20 mV, the values of $\tau_s$ were 5.65 ± 0.15 msec for 'adult' and 6.84 ± 0.24 msec for 'neonatal' ($P < 0.01$; n = 43–37) (Table 1).

### Charge ($Na^+$) entry

The current traces recorded under voltage-clamp (Fig. 3A) suggested that the slower kinetics of the 'neonatal' channel would allow more $Na^+$ influx (i.e. area under the current-time curve is bigger for 'neonatal' than 'adult', at voltages giving same peak current amplitudes; Fig. 3A). Accordingly, we quantified the amount of charge ($Na^+$) entry associated with the 'neonatal' and 'adult' inward currents for the period 0.5 to 30 msec at given voltages (Fig. 3E). Compared to the 'adult', the 'neonatal' channel allowed substantially more $Na^+$ influx, with an overall trend for the difference to increase in the voltage range −30 to +30 mV (Fig. 3E). For example, at 0 mV, the 'neonatal' channel allowed 47% more charge entry into the cell compared to 'adult' isoform (Fig. 3E).

### Time course of recovery from inactivation

Recovery from inactivation was investigated using a double-pulse protocol and best fit with a single exponential function (Fig. 3F). Comparison of the overall fitted data revealed that the recovery time constants (τ) of 'adult' and 'neonatal' splice forms

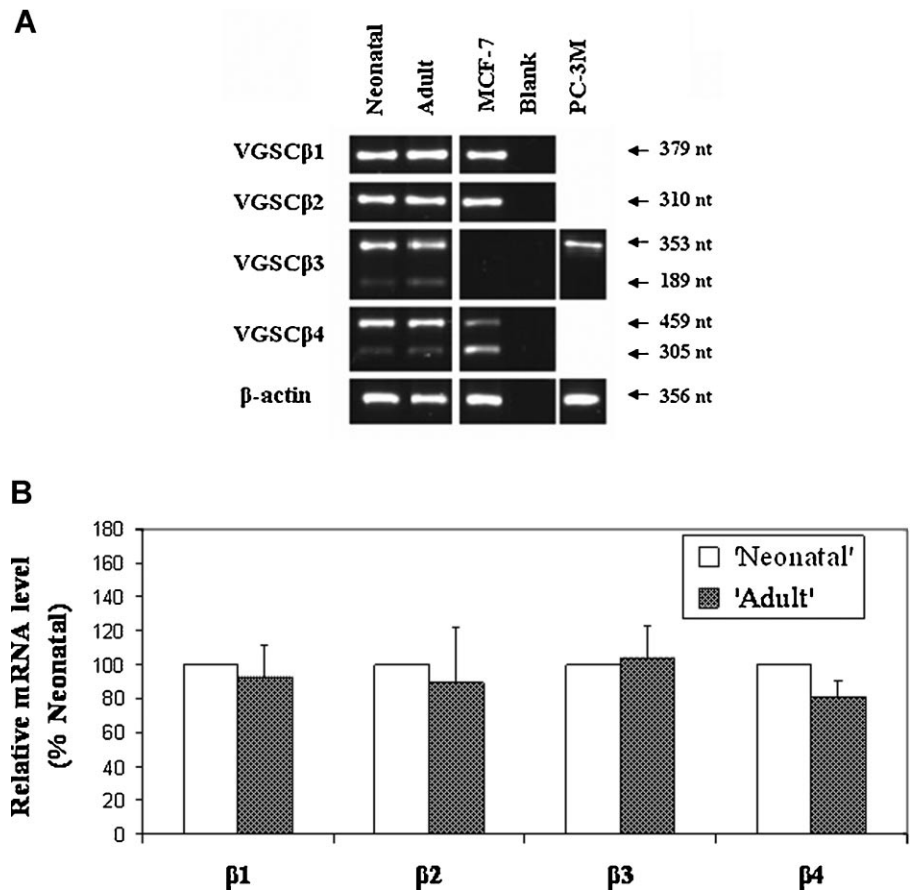


**Fig. 4. VGSCβ mRNA expression in 'adult' and 'neonatal' EBNA-293 cells. A: Typical gel images of PCR products for VGSC β1–4 and β-actin from EBNA-293 cells over-expressing 'neonatal' or 'adult' Nav1.5. MCF-7 (for β1, β2 and β4) and PC-3M (for β3) cell lines were used as controls for primer specificity in real-time PCR experiments. No amplification was evident from the blank controls. B: Real-time PCR data shows that the VGSC β1–4 mRNA levels are similar in 'adult' and 'neonatal' EBNA-293 cell lines. VGSC β1–4 mRNA levels were normalized to β-actin levels using the $2^{-\Delta\Delta C_t}$ method. Data shown are relative to corresponding VGSC β-subunit expression levels in 'neonatal' EBNA-293 cells. Each bar denotes mean ± SEM (n = 3). Data were compared using Student's *t*-test and no statistically significant difference was found.**

differed significantly, with values of 31.2 ± 1.0 and 38.6 ± 0.9 msec, respectively ($P < 0.01$, n = 21–20) (Fig. 3F; Table 1).

### VGSCβ expression in 'adult' versus 'neonatal' Nav1.5 expressing EBNA-293 cells

All four known VGSC β-subunits (β1–4) were expressed in both transfectant cell lines (Fig. 4A). Importantly, the relative mRNA levels of given VGSCβ subtypes were statistically the same for the 'adult' and 'neonatal' EBNA-293 cells ($P > 0.13$, n = 3 each) (Fig. 4B). As controls for primer specificity, we also used MCF-7 and PC-3M cells and confirmed, as shown before, that MCF-7 cells expressed mRNAs for β1, β2 and β4 but not β3, which was present in PC-3M cells (Diss et al., 2007).

### Consequences of K211D mutagenesis on 'neonatal' Nav1.5 electrophysiology

EBNA-293 cells transfected with 'neonatal K211D' Nav1.5 were characterized by patch clamp recording as described above (Fig. 5A). All of the 'neonatal K211D' parameters studied shifted significantly from the 'neonatal' towards 'adult' Nav1.5 values (Figs. 5B,C and 6; Table 1). In the case of the fast inactivation time constant, the shift even overshot the 'adult'

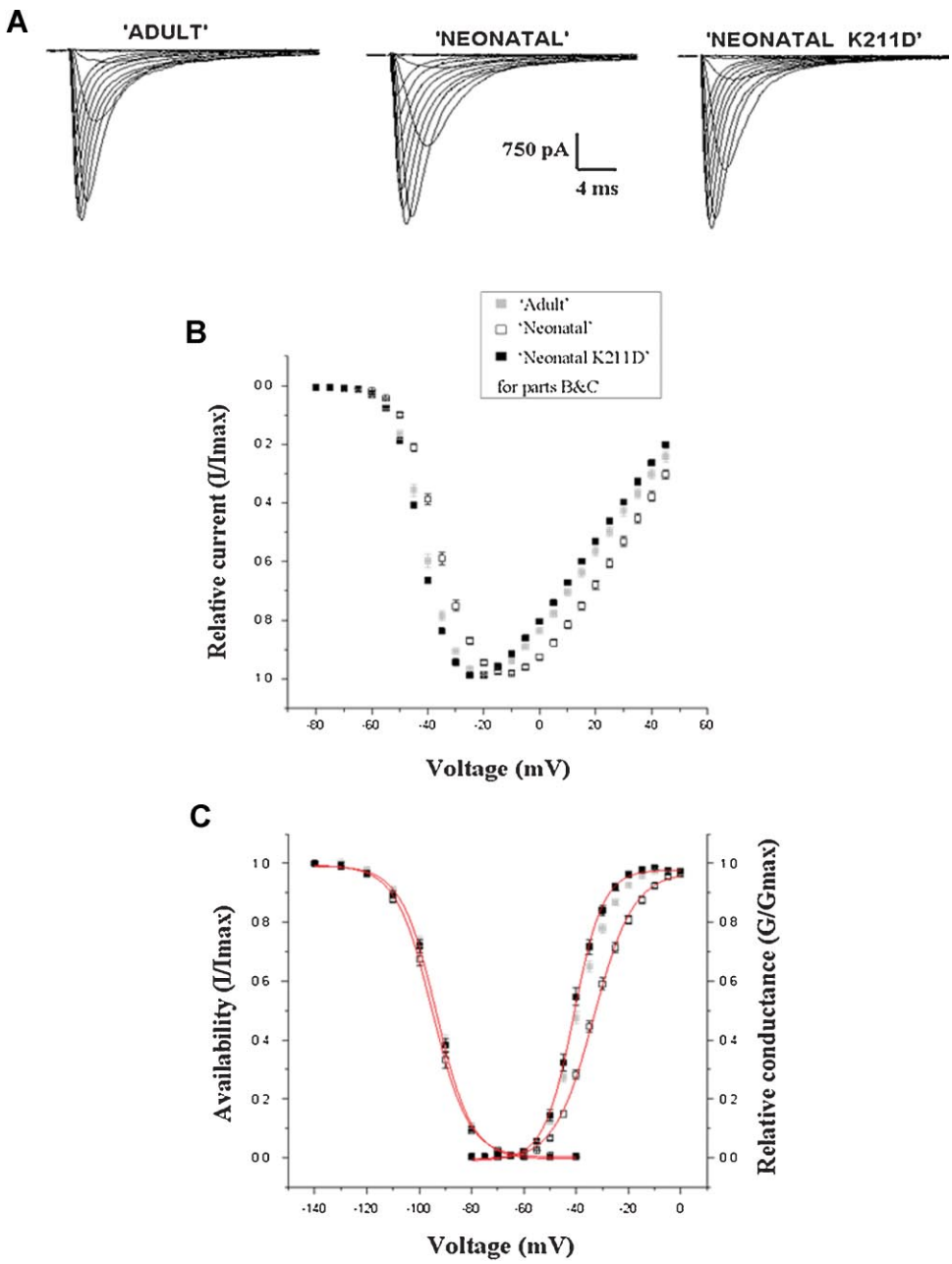


**Fig. 5. Electrophysiological properties of 'neonatal K211D' Nav1.5. A: Representative VGSC current recordings from standard I–V protocol in EBNA-293 cells transfected with 'adult', 'neonatal' and 'neonatal K211D' Nav1.5. For clarity, only every second current trace generated is displayed. B: Normalized peak current versus voltage curves obtained from standard I–V protocol. C: Voltage-dependence of activation and inactivation. Activation conductance and steady state inactivation (availability) were fitted to standard Boltzmann functions. Data are presented as mean ± SEM (n ≥ 20; Table 1).**

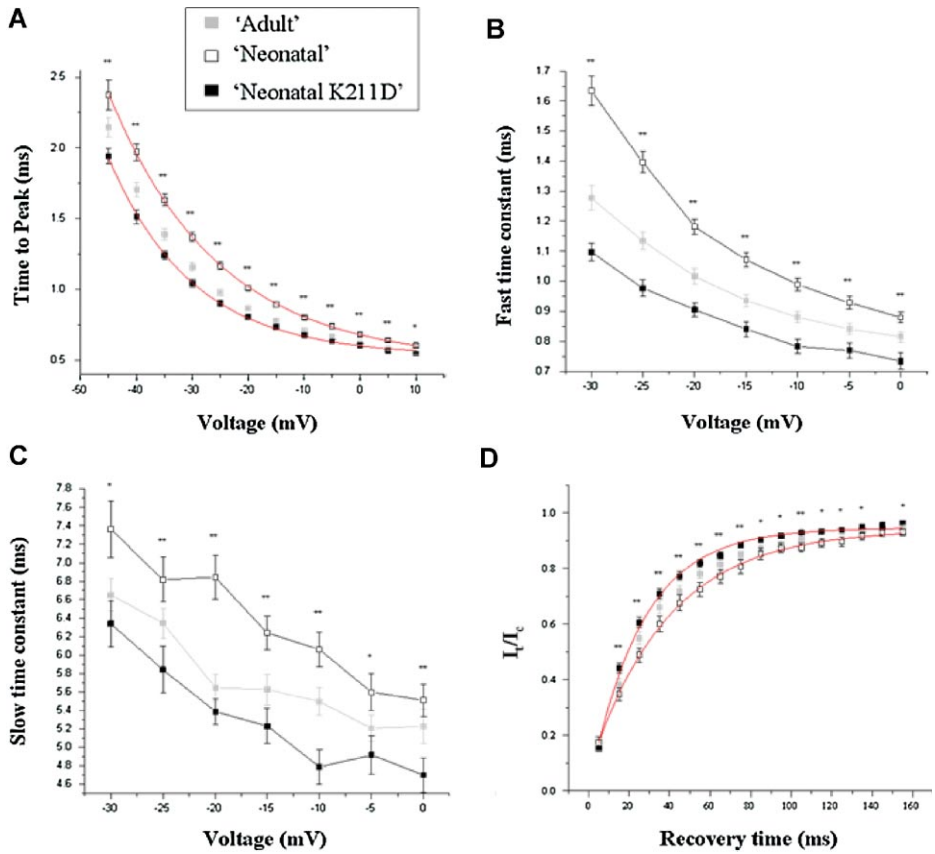


**Fig. 6. Kinetics of 'neonatal K211D' Nav1.5 channel. A: Time to peak, obtained from standard I–V protocol, as a function of test potential and fitted to a single order exponential function. B,C: The fast ($\tau_f$) and slow ($\tau_s$) time constants of inactivation as determined by fitting decaying current curves obtained from the I–V protocol to a double-exponential function. D: Time course of recovery from inactivation. Remaining current ($I_t/I_c$) was plotted as a function of recovery time ($\Delta t$), and fitted to a single exponential function. Data are presented as mean ± SEM ($n \geq 20$; Table 1). Significance $^{*}P < 0.05$ and $^{**}P < 0.01$; unpaired Student's *t*-test comparing 'neonatal' versus 'neonatal K211D' Nav1.5 parameters.**

values (Fig. 6B; Table 1). Partial overshoot was observed for time to peak and recovery from inactivation (Fig. 6A,D; Table 1). An overview comparing the differences in the values of the parameters measured from (1) 'neonatal' Nav1.5 versus 'neonatal K211D'; and (2) 'adult' Nav1.5 versus 'neonatal K211D' is shown in Figure 7. It was clear that mutating the positive lysine residue in 'neonatal' Nav1.5 back to negative aspartate generated a shift consistently towards the 'adult' phenotype.

## Discussion

The main finding of the present study is that the electrophysiological characteristics of the 'neonatal' and the 'adult' splice form of Nav1.5 differed significantly and that a particular amino acid change (aspartate to lysine) in the D1:S3–S3/S4 linker was largely responsible for such differences. Specifically, compared to the 'adult', the 'neonatal' isoform (1) exhibited depolarized values for both activation $V_{1/2}$ and activation k; (2) activated and peaked at a voltage that was ~2 mV and ~7 mV more positive, respectively; (3) possessed a hyperpolarized value for inactivation $V_{1/2}$; (4) had much slower activation and inactivation kinetics; (5) was associated with significantly (~50%) greater $Na^+$ influx; (6) showed a stronger voltage dependence of time to peak; and (7) recovered from inactivation significantly more slowly. VGSCβ mRNA expression levels were similar in EBNA-293 cell lines transfected with either 'adult' and 'neonatal' Nav1.5, which would suggest that the electrophysiological differences found between $Na^+$ currents from these EBNA-293 cell lines did not involve VGSCβs. The K211D mutagenesis in 'neonatal' Nav1.5 resulted in a strong shift from the 'neonatal' back to the 'adult' electrophysiological phenotype. Thus, we concluded that the negative aspartate ('adult') to positive lysine ('neonatal') substitution was primarily responsible for the effects of D1:S3 splicing on Nav1.5 electrophysiology.

### D1:S3 splicing of Nav1.5: functional architecture of VGSC

Our results are consistent with the general trend for ion channels expressed in immature cells having slower kinetics than those in corresponding mature cells (review: Moody and Bosma, 2005). In another study on similar splicing, mainly in D2:S3/S4 of rat Nav1.2, both the voltage-dependence of activation and the voltage for current peak of 'neonatal' isoform were also found to be depolarized 5–10 mV compared to the 'adult' isoform, as reported here (Auld et al., 1990). In addition, although not studied in detail, Auld et al. (1990) reported that the 'neonatal' isoform of rat Nav1.2 exhibited slower 'macroscopic' inactivation, again in agreement with the data reported here for Nav1.5.

The extensive electrophysiological differences between D1:S3 'adult' and 'neonatal' splice variants of Nav1.5 lead us to

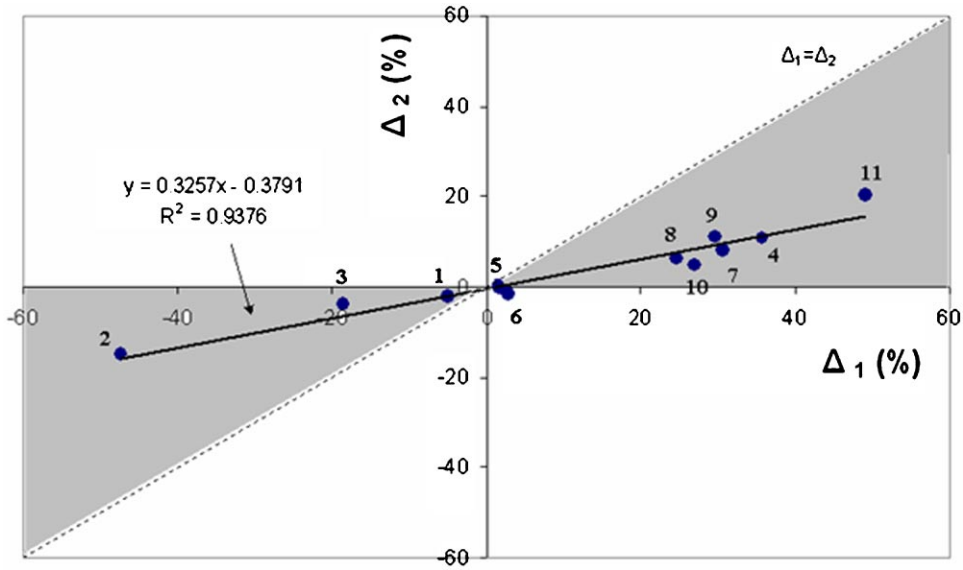


**Fig. 7. Shift from 'neonatal' to 'adult' electrophysiological phenotype following 'neonatal K211D' mutagenesis. Schematic representation of the differences amongst the values of the electrophysiological parameters (from Table 1) recorded from 'neonatal', 'neonatal K211D' and 'adult' Nav1.5. $\Delta_2$ (*y*-axis values) represent the differences between 'neonatal K211D' and 'adult' Nav1.5. $\Delta_1$ (*x*-values) represent the differences between 'neonatal K211D' and 'neonatal' Nav1.5. The numbers adjacent to the data points are for the different parameters measured (as listed in order in Table 1). The dotted line (at 45°) denotes equality (i.e. $\Delta_1 = \Delta_2$). The analysis would indicate that 'neonatal K211D' parameters are closer to 'adult' than 'neonatal' Nav1.5 if the points (i) fell in the shaded region and (ii) were closer to the x-axis. Clearly, both conditions were met (slope of the linear regression, 0.33).**

question the potential significance of the charge-reversing aspartate ('adult') to lysine ('neonatal') substitution at amino acid position 211 (Fig. 1B,C). Switching the lysine back to aspartate resulted in an overall functional shift back towards the 'adult' phenotype (Fig. 7). The critical lysine residue in the 'neonatal' channel might be expected to alter the local electric field sensed by the S4 voltage segment by introducing extra positive electrostatic potential in this region, thereby partially resisting the outward movement of the positively charged S4 segment (Sheets and Hanck, 2002; Henrikson et al., 2003; Chen et al., 2005; McNulty et al., 2007). This is in contrast to the 'adult' channel in which the amino acid residue in this position is a negatively charged aspartate, which is likely to potentiate outward S4 movement by attracting positively charged S4 residues, as reported for the D4:S3–S4 linker mutation V1442E of Nav1.4 (Tsujino et al., 2003).

VGSC kinetics are also known to be affected by association of the α-subunit with auxiliary β-subunit(s) (Isom et al., 1994; Kupershmidt et al., 1998; Isom, 2001; Fahmi et al., 2001; Diss et al., 2004). Accordingly, any difference in endogenous expression levels of VGSCβs in the 'adult' and 'neonatal' Nav1.5-transfected EBNA-293 cells could be a contributing factor to the electrophysiological differences found between the two cell lines. The transfectant EBNA-293 cells were found to be uniform in their VGSCβ mRNA expression levels (Fig. 4). This result further supports our conclusion that it is the lysine/aspartate residue at position 211 that is primarily responsible for the electrophysiological differences found between the 'adult' and 'neonatal' Nav1.5 transfected EBNA-293 cells.

### Possible consequences of D1:S3 alternative splicing

Nav1.5 is the major VGSCα subtype expressed in cardiac muscle (Gellens et al., 1992; Plummer and Meisler, 1999; Catterall, 2000). Immunohistochemical staining of mice tissues showed that 'neonatal' Nav1.5 protein expression is present in hearts of 1 day old pups but completely absent in adults (Chioni et al., 2005). This is consistent with rapid post-partum changes in expression reported previously for Nav1.2 and Nav1.3 splice forms in rat brain (Sarao et al., 1991; Gustafson et al., 1993), and Nav1.4 and Nav1.5 subtypes in rat skeletal muscle (Kallen et al., 1990).

The electrophysiological differences that we have observed between the 'adult' and 'neonatal' isoforms could have a number of physiological (developmental) and pathophysiological consequences. Compared to the 'adult', for example the 'neonatal' channel was associated with a larger charge ($Na^+$) entry into the cell during each opening of the channel. In cardiomyocyte physiology, the additional $Na^+$ influx may be important for intracellular pH regulation, for example via $Na^+$–$H^+$ exchange (reviews: Karmazyn et al., 1999; Bers et al., 2003), activity of key enzymes such as $Na^+/K^+$-ATPase (reviews: Levi et al., 1997; Bers et al., 2003) and protein kinase A (Cooper et al., 1998; Murakami et al., 1998; Brackenbury and Djamgoz, 2006) and $Ca^{2+}$ homeostasis, for example via $Na^+$–$Ca^{2+}$ exchange (review: Blaustein and Lederer, 1999; Pieske and Houser, 2003).

Apart from its electrophysiological effects, the charge-reversing aspartate to lysine change could affect the channel's response to extracellular (intrinsic or extrinsic) chemical factors. Such factors include pH (Khan et al., 2006), which may change under pathophysiological (e.g. ischemic) conditions (Elliott et al., 1992; Watson and Gold, 1995). Splicing in D1:S3 may also have pharmacological implications. Indeed, such splicing of Nav1.1 in humans has been shown to affect the maximum doses that patients can receive of the VGSC-blocking anti-epileptic drugs, carbamazepine and phenytoin, by altering the proportions of the D1:S3 alternative transcripts in these individuals with a history of epilepsy (Tate et al., 2005).

D1:S3 splicing of Nav1.5 may be of pathophysiological importance in heart and brain. For example, it is known that hypertrophied and infracted failing hearts shift to a phenotype characterized by the re-expression of ion channels (e.g. HCN2, HCN4 and CACNA1H) usually restricted to foetal cardiac myocytes (Kuwahara et al., 2003). This is concomitant with the upregulation of the 'neonatal' form of another highly expressed VGSC in heart, Nav1.1 (Huang et al., 2001). Similarly, in the adult brain, 'neonatal' D1:S3 VGSC splicing occurred during seizures induced by kainic acid (Gastaldi et al., 1997). Finally, we have reported upregulation of the 'neonatal' splice form of Nav1.5 in the human metastatic breast cancer cell line MDA-MB-231 and breast biopsy samples (Fraser et al., 2005). Similar expression has been observed in human neuroblastoma cells (Ou et al., 2005). These results are consistent with oncofoetal gene expression during cancer progression (e.g. Ariel et al., 1997; Monk and Holding, 2001). Importantly, activity of the channel in breast cancer potentiated several cellular behaviours linked with metastasis (Fraser et al., 2005; Brackenbury et al., 2007). In overall conclusion, therefore, the electrophysiological characteristics of 'neonatal' Nav1.5 are highly likely to have a number of significant pathophysiological as well as modulatory physiological consequences.

## Literature Cited


Ariel I, Ayesh S, Perlman EJ, Pizov G, Tanos V, Schneider T, Erdmann VA, Podeh D, Komitowski D, Quasem AS, de Groot N, Hochberg A. 1997. The product of the imprinted H19 gene is an oncofetal RNA. Mol Pathol 50:34–44.

Auld VJ, Goldin AL, Krafte DS, Catterall WA, Lester HA, Davidson N, Dunn RJ. 1990. A neutral amino acid change in segment IIS4 dramatically alters the gating properties of the voltage-dependent sodium channel. Proc Natl Acad Sci USA 87:323–327.

Bers DM, Barry WH, Despa S. 2003. Intracellular $Na^+$ regulation in cardiac myocytes. Cardiovasc Res 57:897–912.

Blaustein MP, Lederer WJ. 1999. Sodium/calcium exchange: Its physiological implications. Physiol Rev 79:763–854.

Brackenbury WJ, Djamgoz MB. 2006. Activity-dependent regulation of voltage-gated $Na^+$ channel expression in Mat-LyLu rat prostate cancer cell line. J Physiol 573:343–356.

Brackenbury WJ, Chioni AM, Diss JKJ, Djamgoz MB. 2007. The neonatal splice variant of Nav1.5 potentiates in vitro invasive behaviour of MDA-MB-231 human breast cancer cells. Breast Cancer Res Treat 101:149–160.

Catterall WA. 2000. From ionic currents to molecular mechanisms: The structure and function of voltage-gated sodium channels. Neuron 26:13–25.

Chandra R, Starmer CF, Grant AO. 1998. Multiple effects of KPQ deletion mutation on gating of human cardiac $Na^+$ channels expressed in mammalian cells. Am J Physiol 274:1643–1654.

Chen T, Inoue M, Sheets MF. 2005. Reduced voltage dependence of inactivatation in the SCN5A sodium channel mutation del F1617. Am J Physiol Heart Circ Physiol 288:2666–2676.

Chioni AM, Fraser SP, Pani F, Foran P, Wilkin GP, Diss JKJ, Djamgoz MB. 2005. A novel polyclonal antibody specific for the Nav1.5 voltage-gated $Na^+$ channel 'neonatal' isoform. J Neurosci Methods 147:88–98.

Cooper DM, Schell MJ, Thorn P, Irvine RF. 1998. Regulation of adenylyl cyclase by membrane potential. J Biol Chem 273:27703–27707.

Dietrich PS, McGivern JG, Delgado SG, Koch BD, Eglen RM, Hunter JC, Sangameswaran L. 1998. Functional analysis of a voltage-gated sodium channel and its splice variant from rat dorsal root ganglia. J Neurochem 70:2262–2272.

Diss JKJ, Fraser SP, Djamgoz MB. 2004. Voltage-gated $Na^+$ channels: Functional consequences of multiple subtypes and isoforms for physiology and pathophysiology. Eur Biophys J 33:180–193.

Diss JK, Stewart D, Pani F, Foster CS, Walker MM, Patel A, Djamgoz MB. 2005. A potential novel marker for human prostate cancer: Voltage-gated sodium channel expression in vivo. Prostate Cancer Prostatic Dis 8:266–273.

Diss JK, Fraser SP, Walker MM, Patel A, Latchman DS, Djamgoz MB. 2007. Beta-subunits of voltage-gated sodium channels in human prostate cancer: Quantitative in vitro and in vivo analyses of mRNA expression. Prostate Cancer Prostatic Dis [Epub ahead of print—September 25].

Elliott AC, Smith GL, Eisner DA, Allen DG. 1992. Metabolic changes during ischaemia and their role in contractile failure in isolated ferret hearts. J Physiol 454:467–490.

Fahmi AI, Patel M, Stevens EB, Fowden AL, John JE III, Lee K, Pinnock R, Morgan K, Jackson AP, Vandenberg JI. 2001. The sodium channel beta-subunit SCN3b modulates the kinetics of SCN5a and is expressed heterogeneously in sheep heart. J Physiol 537:693–700.

Fraser SP, Diss JKJ, Chioni AM, Mycielska ME, Pan H, Yamaci RF, Pani F, Siwy Z, Krakowska M, Grzywna Z, Brackenbury WJ, Theodorou D, Koyutürk M, Kaya H, Battaloğlu E, Tamburo De Bella M, Slade MJ, Tolhurst R, Palmieri C, Jiang J, Latchman DS, Coombes RC, Djamgoz MB. 2005. Voltage-gated sodium channel expression and potentiation of human breast cancer metastasis. Clin Cancer Res 11:5381–5389.

Gastaldi M, Bartolomei F, Massacrier A, Planells R, Robaglia-Schlupp A, Cau P. 1997. Increase in mRNAs encoding neonatal II and III sodium channel alpha-isoforms during kainate-induced seizures in adult rat hippocampus. Brain Res Mol Brain Res 44:179–190.

Gellens ME, George AL Jr, Chen LQ, Chahine M, Horn R, Barchi RL, Kallen RG. 1992. Primary structure and functional expression of the human cardiac tetrodotoxin-insensitive voltage-dependent sodium channel. Proc Natl Acad Sci USA 89:554–558.

Grimes JA, Fraser SP, Stephens GJ, Downing JEG, Laniado ME, Foster CS, Abel PD, Djamgoz MB. 1995. Differential expression of voltage-activated $Na^+$ currents in two prostatic tumour cell lines: Contribution to invasiveness in vitro. FEBS Lett 369:290–294.

Gustafson TA, Clevinger EC, Oneill TJ, Yarowsky PJ, Krueger BK. 1993. Mutually exclusive exon splicing of type-III brain sodium channel-alpha subunit RNA generates developmentally-regulated isoforms in rat-brain. J Biol Chem 268:18648–18653.

Henrikson CA, Xue T, Dong P, Sang D, Marban E, Li RA. 2003. Identification of a surface charged residue in the S3-S4 linker of the pacemaker (HCN) channel that influences activation gating. J Biol Chem 278:13647–13654.

Huang B, El-Sherif T, Gidh-Jain M, Qin D, El-Sherif N. 2001. Alterations of sodium channel kinetics and gene expression in the postinfarction remodeled myocardium. J Cardiovasc Electrophysiol 12:218–225.

Isom LL. 2001. Sodium channel β subunits: Anything but auxiliary. Neuroscientist 7:42–54.

Isom LL, De Jongh KS, Catterall WA. 1994. Auxiliary subunits of voltage-gated ion channels. Neuron 12:1183–1194.

Kallen RG, Sheng ZH, Yang J, Chen LQ, Rogart RB, Barchi RL. 1990. Primary structure and expression of a sodium channel characteristic of denervated and immature rat skeletal muscle. Neuron 4:233–242.

Karmazyn M, Gan XT, Humphreys RA, Yoshida H, Kusumoto K. 1999. The myocardial $Na^+$-$H^+$ exchange: Structure, regulation and its role in heart disease. Circ Res 85:777–786.

Khan A, Kyle JW, Hanck DA, Lipkind GM, Fozzard HA. 2006. Isoform-dependent interaction of voltage-gated sodium channels with protons. J Physiol 576:493–501.

Klugbauer N, Lacinova L, Flockerzi V, Hofmann F. 1995. Structure and functional expression of a new member of the tetrodotoxin-sensitive voltage-activated sodium-channel family from human neuroendocrine cells. EMBO J 14:1084–1090.

Kupershmidt S, Yang T, Roden DM. 1998. Modulation of cardiac $Na^+$ current phenotype by beta1-subunit expression. Circ Res 83:441–447.

Kuwahara K, Saito Y, Takano M, Arai Y, Yasuno S, Nakagawa Y, Takahashi N, Adachi Y, Takemura G, Horie M, Miyamoto Y, Morisaki T, Kuratomi S, Noma A, Fujiwara H, Yoshimasa Y, Kinoshita H, Kawakami R, Kishimoto I, Nakanishi M, Usami S, Saito Y, Harada M, Nakao K. 2003. NRSF regulates the fetal cardiac gene program and maintains normal cardiac structure and function. EMBO J 22:6310–6321.

Levi AJ, Dalton GR, Hancox JC, Mitcheson JS, Issberner J, Bates JA, Evans SJ, Howarth FC, Hobai IA, Jones JV. 1997. Role of intracellular sodium overload in the genesis of cardiac arrhythmias. J Cardiovasc Electrophysiol 6:700–721.

Livak KJ, Schmittgen TD. 2001. Analysis of relative gene expression data using real-time quantitative PCR and the 2(-Delta Delta C(T)) Method. Methods 25:402–408.

McNulty MM, Edgerton GB, Shah RD, Hanck DA, Fozzard HA, Lipkind GM. 2007. Charge at the lidocaine binding site residue Phe-1759 affects permeation in human cardiac voltage-gated sodium channels. J Physiol 581:741–755.

Monk M, Holding C. 2001. Human embryonic genes re-expressed in cancer cells. Oncogene 20:8085–8091.

Moody WJ, Bosma MM. 2005. Ion channel development, spontaneous activity, and activity-dependent development in nerve and muscle cells. Physiol Rev 85:883–941.

Murakami Y, Tanaka J, Koshimura K, Kato Y. 1998. Involvement of tetrodoxin-sensitive sodium channels in rat growth hormone secretion induced by pituitary adenylate cyclase-activating polypeptide (PACAP). Regul Pept 73:119–121.

Mycielska ME, Palmer CP, Brackenbury WJ, Djamgoz MB. 2005. Expression of $Na^+$-dependent citrate transport in a strongly metastatic human prostate cancer PC-3M cell line: Regulation by voltage-gated $Na^+$ channel activity. J Physiol 563:393–408.

Ou SW, Kameyama A, Hao LY, Horiuchi M, Minobe E, Wang WY, Makita N, Kameyama M. 2005. Tetrodotoxin-resistant $Na^+$ channels in human neuroblastoma cells are encoded by new variants of Nav1.5/SCN5A. Eur J Neurosci 22:793–801.

Pieske B, Houser SR. 2003. $[Na^+]_i$ handling in the failing human heart. Cardiovasc Res 57:874–886.

Plummer NW, Meisler MH. 1999. Evolution and diversity of mammalian sodium channel genes. Genomics 57:323–331.

Plummer NW, Galt J, Jones JM, Burgess DL, Sprunger LK, Kohrman DC, Meisler MH. 1998. Exon organization, coding sequence, physical mapping, and polymorphic intragenic markers for the human neuronal sodium channel gene SCN8A. Genomics 54: 287–296.

Raymond CK, Castle J, Garrett-Engele P, Armour CD, Kan Z, Tsinoremas N, Johnson JM. 2004. Expression of alternatively spliced sodium channel alpha-subunit genes: Unique splicing patterns are observed in dorsal root ganglia. J Biol Chem 279:46234–46241.

Sarao R, Gupta SK, Auld VJ, Dunn RJ. 1991. Developmentally regulated alternative RNA splicing of rat-brain sodium-channel messenger-RNAs. Nucleic Acids Res 19:5673–5679.

Schaller KL, Krzemien DM, Yarowsky PJ, Krueger BK, Caldwell JH. 1995. A novel, abundant sodium channel expressed in neurons and glia. J Neurosci 15:3231–3242.

Sheets MF, Hanck DA. 2002. The outermost lysine in the S4 of domain III contributes little to the gating charge in sodium channels. Biophys J 82:3048–3055.

Tate SK, Depondt C, Sisodiya SM, Cavalleri GL, Schorge S, Soranzo N, Thom M, Sen A, Shorvon SD, Sander JW, Wood NW, Goldstein DB. 2005. Genetic predictors of the maximum doses patients receive during clinical use of the anti-epileptic drugs carbamazepine and phenytoin. Proc Natl Acad Sci USA 102:5507–5512.

Tsujino A, Maertens C, Ohno K, Shen XM, Fukuda T, Harper CM, Cannon SC, Engel AG. 2003. Myasthenic syndrome caused by mutation of the SCN4A sodium channel. Proc Natl Acad Sci USA 100:7377–7382.

Watson CL, Gold MR. 1995. Effect of intacellular and extracellular acidosis on sodium current in ventricular myocytes. Am J Physiol 268:1749–1756.

Xiao YF, Wright SN, Wang GK, Morgan JP, Leaf A. 2000. Coexpression with beta(1)-subunit modifies the kinetics and fatty acid block of hH1 (alpha) Na(+) channels. Am J Physiol Heart Circ Physiol 279:35–46.